Contributions, Geophysical Institute, Kyoto University, No. 13, 1973, 163–169

INVESTIGATIONS OF FINE STRUCTURE OF THE CORE-MANTLE INTERFACE BY DIFFRACTED SH WAVES —A PRELIMINARY REPORT—

By

Akio Sakai

(Received September 3, 1973)

Abstract

Seismic waves of six intermediate or deep earthquakes are Fourier-analysed selecting stations of the distance beyond 90 degrees.

From the observed relation between logarithmic amplitude spectra of SH waves and distance, we introduced an apparent attenuation function $\gamma(\omega)$. It is found that the absolute value of γ and the troughs at 0.03 to 0.04 Hz and 0.08 to 0.09 Hz are similar to each event.

1. Introduction

Although many researchers attempted to elucidate the fine structure—density, elastic and anelastic properties—of the Earth's Core-Mantle interface, definite answers have not yet been derived. Furthermore, the problem of lateral inhomogeneity concerning bumps or hot spots arises mostly from observations of gravity and geomagnetism.

It is most straightforward to analyse seismic body waves transmitted through the interface; grazing ray or diffracted waves by the Core (ALEXANDER AND PHINNEY (1966)). We use diffracted SH waves with the intention of degenerating the equations of motion and boundary conditions, and calculate the frequency-dependent attenuation function near the geometrical shadow point.

2. Analysis and discussions

We select suitable events referring to ISACKS AND MOLNAR (1971) and MIKUMO (1971), and derive seismic data of long-period seismograms (T_1=15–30sec, T_2=90–100 sec) from WWSSN. The concerned parameters are listed on Table 1.

We assumed a linear filter system as below.

$$aP_o(\omega)\rightarrow P_{M_1}(\omega)\rightarrow P_{MCB}(\omega)\rightarrow P_{M_2}(\omega)\rightarrow P_I(\omega)$$

where a is the spatial term and $P_o(\omega)$ the frequency dependent term due to the source time function, $P_{M_1}(\omega)$ the frequency response of a ray path from a source down to the

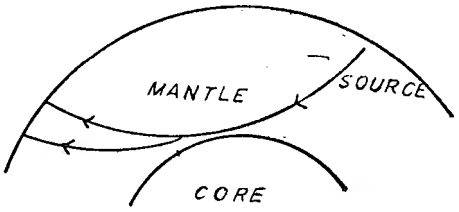

Fig. 1. Paths of observed rays

base of the Mantle, $P_{MCB}(\omega)$ the response of a diffracted wave or a ray grazing the Earth's Core, $P_{M_2}(\omega)$ the response of a ray path from the base of the Mantle up to an Earth's surface and $P_I(\omega)$ the instrumental response. (See Fig. 1)

When the corrected amplitude of the k-th station by terms of a, $P_o(\omega)$ and $P_I(\omega)$ is expressed as $A^{(k)}_{\text{cor.}}(\omega)$ and $P_{MCB}(\omega)$ of the k-th station as $P^{(k)}_{MCB}(\omega)$.

$$\frac{P^{(k)}_{MCB}(\omega)}{P^{(i)}_{MCB}(\omega)} = \frac{A^{(k)}_{\text{cor.}}(\omega)}{A^{(i)}_{\text{cor.}}(\omega)} \tag{1}$$

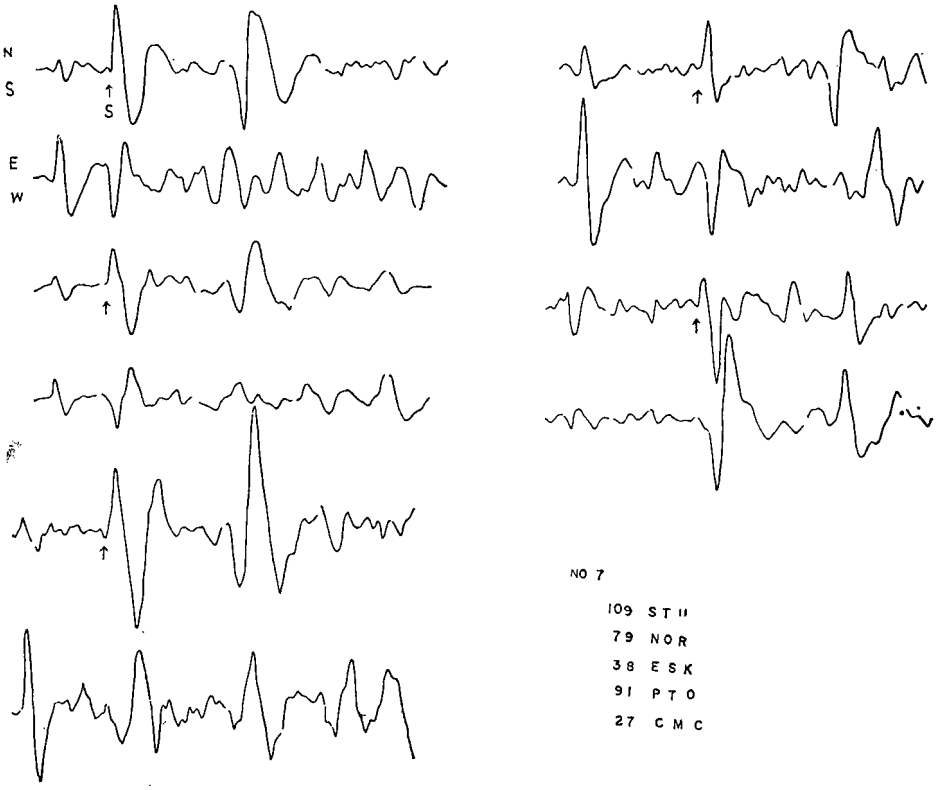

Fig. 2. Examples of waveform (event No. 7)

We give an illustration of waveforms with adjacent phases such as SKS, SKKS and pS from events No. 7, for instance, in Fig. 2.

The Fourier transform is performed in the frequency range between 0.01 and 0.15 Hz, with the time window, truncated length and digitized interval;

$$\left.\begin{aligned} W(t) &= 0.54+0.46\cos(\pi t/T) \\ T &= 30 \text{ sec–}60 \text{ sec} \\ \Delta t &= 0.5 \text{ sec–}1.2 \text{ sec} \end{aligned}\right\} \tag{2}$$

respectively.

The example of Fourier spectra of amplitudes and phases is illustrated in Fig. 3 from event No. 4.

The frequencies for peaks and troughs of the amplitude spectra nearly correspond with those of the phase spectra. This could be explained by the effects of finite dimension of sources or partly, of contamination of preceded and later phases. It is noticeable that there are no systematic transitions of the peaks and troughs of the amplitudes and phase spectra with increasing epicentral distances in all events. The instanced amplitude spectra of event No. 4 appear to be divided into some classes, which might be related to the finite dimension of the source and complex source process.

The logarithms of amplitudes of events No. 4 and No. 7 at 0.05 Hz are plotted against distances in Fig. 4, after normalizing the spectra at a distance of 90 degrees. It is observable that the amplitudes tend to decline linearly with increasing distances beyond 93 to 95 degrees, and that around 90 degrees are some fluctuations, which is possibly attributed to the interference of S and ScS. Hence we introduce an apparent attenuation function γ determined by the decline of the amplitude; $\exp(-\gamma\cdot\Delta)$, where Δ is the epicentral distance.

By least square method, the function $\gamma(\omega)$ is fitted in each of events.

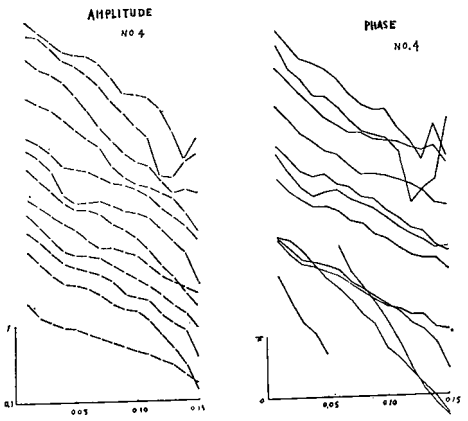

Fig. 3. Examples of amplitude spectra and phase spectra (event No. 4)

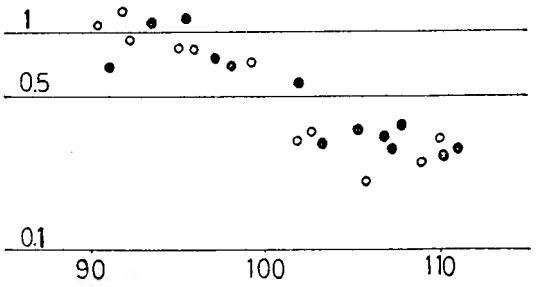

Fig. 4. Logarithmic amplitude spectra No. 4 (closed circle) and No. 7 (open circle) at 0.05 Hz to base ten.

The calculated γ's are illustrated with estimated standard errors, in Fig. 5, where the dimension of γ is [1/deg].

The trend of γ's in events No. 1 and No. 7 has similarity with each other, including the absolute value of γ's. Event No. 6 belongs to the above group, except the absolute value, and we can say that for higher frequencies γ in events No. 6 and No. 8 is similar. However we cannot get any meaningful value of γ for event No. 5, owing to large standard errors. The reason for this might be attributed to inappropriate combination of stations due to some allowance for the fault plane solutions and/or trapping of seismic energy within a seismic zone near the source region. It should be remarked that the distance ranges of the stations used are somewhat different; 95 to 110 degrees for events No. 1, No. 4 and No. 7, 95 to 117 degrees for events No. 6 and No. 8, 95 to 114 degrees for event No. 5.

In spite of some differences in the absolute value of γ, a trough around 0.08 to 0.09 Hz is most remarkable in common, and that a trough around 0.03 to 0.04 Hz is next remarkable, except event No. 1. It is very interesting that these features appear to suggest the existence of a "gallery" through which seismic waves transmit selectively.

Further we should add that the effect of the upper limit of the distance ranges could not be disregarded, contrasting events No. 6 and No. 8 with the others. A probable elucidation is that the deeper is the upper limit of the distances, the worse the SN ratio is, while closer examinations of Fig. 4 suggest that the amplitudes become saturated gradually.

References

Alexander, S. S. and R. A. Phinney, A study of the core-mantle boundary using P waves diffracted by the earth's core, J. Geophys. Res., 71, 5943–5958, 1966

Isacks, B. and P. Molnar, Distribution of stresses in the descending lithosphere from a global survey of focal-mechanism solutions of mantle earthquakes, Reviews of Geophys. and Space Phys., 9, No. 1, 103–174, 1971.

Mikumo, T., Source process of deep and intermediate earthquakes as inferred from long-period P and S waveforms 2. deep-focus and intermediate-depth earthquakes around Japan, J. Phys. Earth, 19, No. 4, 303–320, 1971.

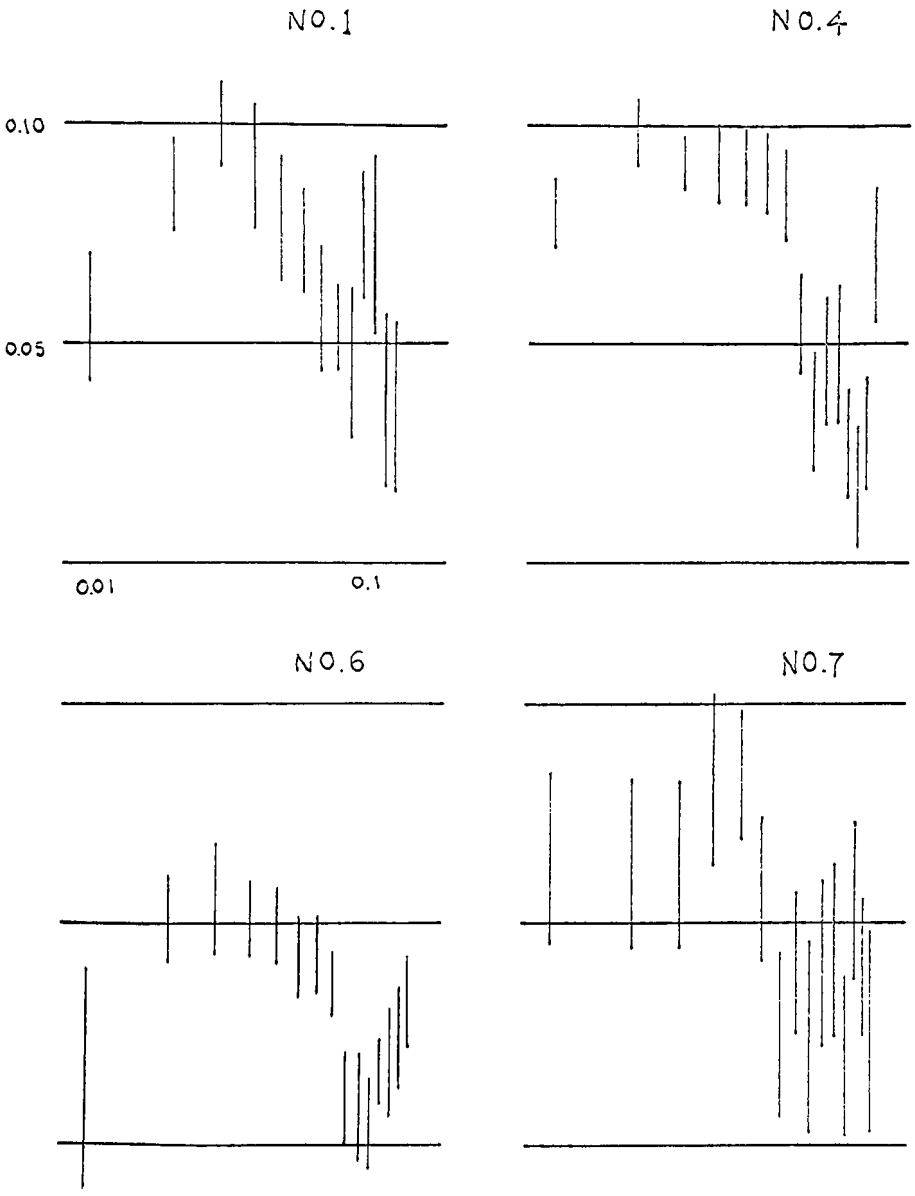
NO.1
NO.4
0.10
0.05
0.01
0.1
NO.6
NO.7

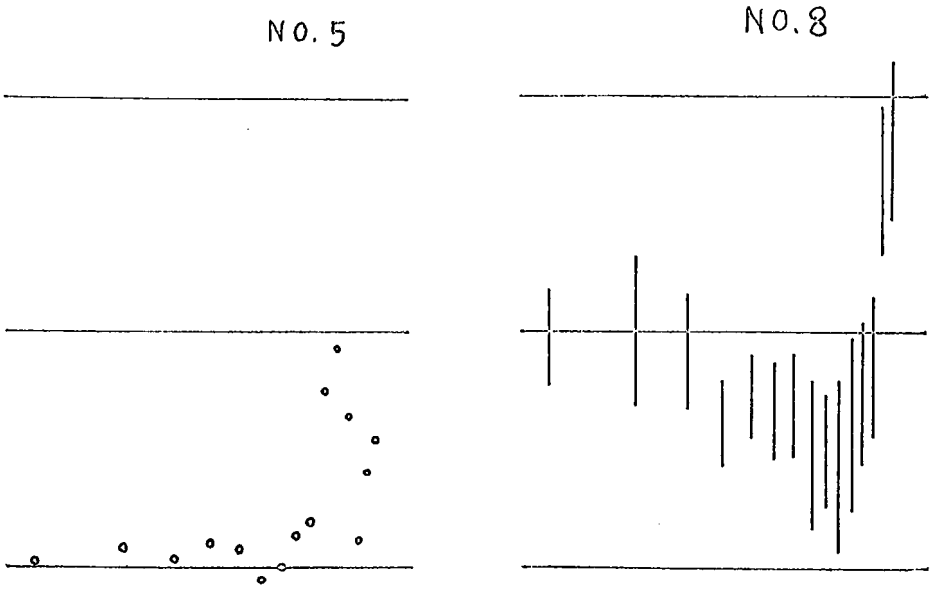

Fig. 5. Relations between γ and logarithmic frequency with estimated standard errors.

Table 1. Analysed earthquakes, referred stations of WWSSN in each event. (Referred papers: event No. 1, MIKUMO (1971); events Nos. 4, 5, 6, 7 and 8, ISACKS AND MOLNAR (1971))

Station	Distance	Azimuth (from focus)	Azimuth (at station)
No. 1			
85 GSC	90.07	307.39	48.45
74 NAI	92.88	60.29	270.19
43 GOL	94.07	317.67	39.18
119 TUC	95.85	310.77	47.61
7 ALQ	96.76	313.64	43.21
65 MAL	100.83	39.64	323.82
2 AAM	101.97	331.04	24.44
39 FLO	102.24	325.36	30.76
123 WES	105.59	341.40	15.79
83 OXF	106.21	325.48	32.61
19 BLA	107.63	333.06	24.62
12 ATL	109.38	329.25	29.50
103 SHA	109.95	325.74	33.94
15 EEC	116.64	346.33	13.32
No. 4			
85 GSC	91.45	307.42	47.87
96 RCD	93.41	313.69	34.36
43 GOL	95.42	314.93	38.58
119 TUC	97.22	310.82	47.01
7 ALQ	98.13	313.79	42.61
63 LUB	101.77	313.68	40.83
2 AAM	103.22	331.65	23.72
35 JCT	105.23	317.57	41.68
123 WES	106.73	342.20	14.98
82 OGD	107.15	339.17	17.87
83 OXF	107.52	325.90	31.90
12 ATL	110.68	329.76	28.73
89 PRE	110.23	66.83	251.17
No. 5			
18 BKS	85.86	242.23	47.74
85 GSC	88.66	245.66	51.97
58 LON	90.28	242.26	40.03
36 DUG	93.49	248.16	48.72
7 ALQ	96.42	251.44	55.40
43 GOL	98.71	252.67	51.11
27 CMC	102.28	249.99	22.14
9 ANT	108.26	238.96	123.89
78 NNA	108.28	245.30	110.04
39 FLO	109.85	261.26	54.71
11 ARE	110.94	241.74	116.72
60 LUB	113.75	240.11	118.49
No. 6			
28 COL	92.43	261.81	25.10
47 HLW	99.14	91.36	299.22
52 KEV	99.37	81.08	339.78
79 NOR	102.63	35.50	355.08
120 UME	103.20	75.90	334.38
27 CMC	105.02	292.57	20.63
13 ATH	105.26	85.33	305.66
29 COP	109.31	71.10	327.42
55 KON	109.30	67.25	331.92
109 STU	113.40	70.92	321.07
40 GDH	116.56	357.63	0.86
38 ESK	117.45	56.67	331.32
No. 7			
29 COP	90.29	91.33	325.51
55 KON	91.80	88.90	329.43
109 STU	92.22	88.99	318.58
79 NOR	94.97	62.21	352.52
126 LOR	95.93	85.06	317.26
38 ESK	99.17	78.41	325.94
100 KTG	101.67	58.38	343.31
115 TOL	102.55	80.70	310.58
91 PTO	105.72	77.27	312.54
27 CMC	108.71	321.01	13.80
40 GDH	109.83	26.66	350.79
No. 8			
7 ALQ	88.62	242.13	51.69
28 COL	89.04	209.11	12.84
26 CHG	89.37	112.41	290.31
22 BOZ	90.24	239.67	40.46
43 GOL	91.52	243.79	47.83
35 JCT	91.82	246.69	58.10
96 RCD	94.86	245.41	44.57
61 LPB	95.05	249.64	76.71
78 NNA	96.98	246.80	105.80
27 CMC	100.14	238.58	20.29
103 SHA	101.31	252.22	61.44
83 OXF	101.45	252.34	57.41
60 LPB	102.77	243.32	113.41
67 MDS	103.75	254.03	48.65
12 ATL	105.19	254.63	59.70
21 BOG	105.75	249.51	91.08
54 KOD	105.99	109.06	274.99
87 POO	111.81	105.82	282.19
82 OGD	114.30	262.64	53.42
123 WES	116.89	265.33	116.89

No. 1 1968 May 14 D=168km Mb=5.9
14h 5m 6.04s/29.93N 129.37E
No. 4 1965 Sept. 21 D=195km Mb=6.0
1h 36m 30.3s/28.96N 128.23E
No. 5 1963 May 1 D=142km Mb=6.8
10h 3m 20.0s/19.0S 168.9E
No. 6 1965 Aug. 20 D=328km Mb=6.1
5h 54m 50.6s/5.74S 128.63E
No. 7 1967 May 21 D=173km Mb=6.3
18h 45m 11.7s/0.97S 101.47E
No. 8 1966 Mar. 17 D=626km Mb=6.2
15h 50m 32.2s/21.08S 179.18W